SERIES IN OPTICS AND OPTOELECTRONICS

Optical Microring Resonators

Theory, Techniques, and Applications

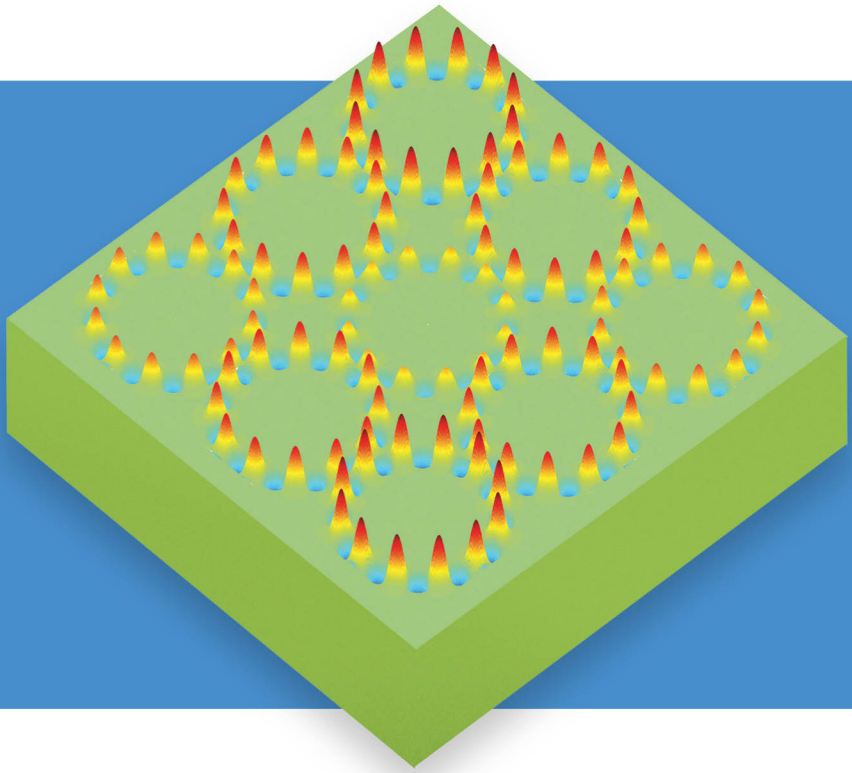

V. Van

CRC Press
Taylor & Francis Group
A TAYLOR & FRANCIS BOOK

Optical Microring Resonators

Theory, Techniques, and Applications

SERIES IN OPTICS AND OPTOELECTRONICS

Recent titles in the series

Optical Microring Resonators: Theory, Techniques, and Applications
V. Van

Optical Compressive Imaging
Adrian Stern

Singular Optics
Gregory J. Gbur

The Limits of Resolution
Geoffrey de Villiers and E. Roy Pike

Polarized Light and the Mueller Matrix Approach
José J Gil and Razvigor Ossikovski

Light—The Physics of the Photon
Ole Keller

Advanced Biophotonics: Tissue Optical Sectioning
Ruikang K Wang and Valery V Tuchin (Eds.)

Handbook of Silicon Photonics
Laurent Vivien and Lorenzo Pavesi (Eds.)

Microlenses: Properties, Fabrication and Liquid Lenses
Hongrui Jiang and Xuefeng Zeng

Laser-Based Measurements for Time and Frequency Domain Applications: A Handbook
Pasquale Maddaloni, Marco Bellini, and Paolo De Natale

Handbook of 3D Machine Vision: Optical Metrology and Imaging
Song Zhang (Ed.)

Handbook of Optical Dimensional Metrology
Kevin Harding (Ed.)

Biomimetics in Photonics
Olaf Karthaus (Ed.)

Optical Properties of Photonic Structures: Interplay of Order and Disorder
Mikhail F Limonov and Richard De La Rue (Eds.)

Nitride Phosphors and Solid-State Lighting
Rong-Jun Xie, Yuan Qiang Li, Naoto Hirosaki, and Hajime Yamamoto

Optical Microring Resonators

Theory, Techniques, and Applications

V. Van
University of Alberta
Edmonton, Canada

CRC Press
Taylor & Francis Group
Boca Raton London New York

CRC Press is an imprint of the
Taylor & Francis Group, an **informa** business
A TAYLOR & FRANCIS BOOK

CRC Press
Taylor & Francis Group
6000 Broken Sound Parkway NW, Suite 300
Boca Raton, FL 33487-2742

Printed on acid-free paper
Version Date: 20161004

International Standard Book Number-13: 978-1-4665-5124-4 (Hardback)

Library of Congress Cataloging-in-Publication Data

Names: Van, Vien, 1971- author.
Title: Optical microring resonators : theory, techniques, and applications / Vien Van.
Other titles: Series in optics and optoelectronics (CRC Press)
Description: Boca Raton, FL : CRC Press, Taylor & Francis Group, [2017] |
Series: Series in optics and optoelectronics
Identifiers: LCCN 2016040265| ISBN 9781466551244 (hardback ; alk. paper) | ISBN 1466551240 (hardback ; alk. paper)
Subjects: LCSH: Microresonators (Optoelectronics) | Optoelectronic devices. | Optical wave guides. | Nonlinear optics.
Classification: LCC TK8360.M53 V36 2017 | DDC 621.381/045--dc23
LC record available at https://lccn.loc.gov/2016040265

Visit the Taylor & Francis Web site at
http://www.taylorandfrancis.com

and the CRC Press Web site at
http://www.crcpress.com

Contents

Preface

Since their early development in the 1990s, optical microring resonators have become one of the most important elements in integrated optics technology. These simple but versatile structures have found myriad applications in filters, sensors, lasers, nonlinear optics, optomechanics, and more recently, quantum optics. Indeed, it is difficult to imagine an integrated photonic system today that does not utilize a microring resonator as part of the circuit architecture. Given the diversity and ubiquitousness of their applications, the need arises for a systematic review of the technology that can serve as a reference source for engineers and researchers working in the broader field of integrated photonics.

The objective of this book is to provide a concise treatment of the theory, principles and techniques of microring resonator devices, and their applications. It is intended for graduate students and researchers who wish to familiarize themselves with the technology and acquire sufficient knowledge to enable them to design microring devices for their own applications of interest. Rapid advances in integrated optics and microfabrication technologies have enabled microring devices with increasingly more sophisticated designs and superior performance to be developed. However, the underlying working principles of these devices remain the same for the most part. Thus, while attempts are made to highlight some of the recent advances in microring technology, the main focus of the book is to provide a detailed treatment of the underlying theory and techniques for modeling and designing microring devices so that the reader can readily apply the knowledge to their own applications. Toward this aim, numerous numerical examples are given to help illustrate the application of these techniques, as well as to demonstrate what can theoretically be achieved with these devices. Many of the examples are based on the silicon-on-insulator material system, a choice motivated by the growing prevalence of silicon photonics in integrated optics technology.

The book is divided into five chapters. While a basic familiarity with optics is assumed, a brief review of the concepts essential to

the understanding of microring resonators and their applications will be given in the relevant chapters. In particular, Chapter 1 will give a review of the theory of optical waveguides, whispering gallery modes, and coupled waveguide systems, which are the basic elements constituting any microring device. Chapter 2 develops the basic formalisms used to analyze simple microring resonators coupled to one or more waveguides. Chapter 3 is devoted to the analysis and design of coupled microring resonators for filter applications. Nonlinear optics and active photonic applications of microring resonators are the subjects of Chapters 4 and 5, respectively.

This book is born out of my research on microring resonators which began at the University of Waterloo, Ontario, Canada, in the late 1990s and subsequently at the University of Maryland, College Park, in the early 2000s. I have in particular benefited tremendously from the mentorship of Professor Ping-Tong Ho as well as from my colleagues at the Laboratory for Physical Sciences at the University of Maryland. The contributions of my graduate students at the University of Alberta have also helped shape a large part of this book, with special acknowledgment to Ashok Prabhu Masilamani, Alan Tsay, Daniel Bachman, Guangcan Mi, and Siamak Abdollahi. I also acknowledge the assistance of many students in the preparation and editing of the book, with special thanks to Jocelyn Bachman, Guangcan Mi, Yang Ren, and Daniel Bachman for reviewing and proofreading parts of the manuscript.

V. Van
University of Alberta
September 2016

CHAPTER 1

Elements of an Optical Microring Resonator

An optical microring resonator is an integrated optic traveling wave resonator constructed by bending an optical waveguide to form a closed loop, typically of a circular or racetrack shape. Light propagating in the microring waveguide interferes with itself after every trip around the ring. When the roundtrip length is exactly equal to an integer multiple of the guided wavelength, constructive interference of light occurs which gives rise to sharp resonances and large intensity buildup inside the microring. The high wavelength selectivity, strong dispersion, large field enhancement, and high quality factor are important characteristics which make microring resonators extremely versatile and useful for a wide range of applications in optical communication, signal processing, sensing, nonlinear optics and, more recently, quantum optics.

Microring and microdisk resonators were first proposed by Marcatili in 1969 for realizing channel dropping filters based on planar optical waveguides (Marcatili 1969b). Similar traveling wave filters based on microwave striplines had been proposed and studied earlier by Coale (1956). However, it was not until the late 1990s that advances in the microfabrication technology for integrated photonic devices enabled optical microring resonators to be realized with high quality factors. Since then, microring and microdisk resonators have been demonstrated for a wide range of applications in various material systems such as silicon-on-insulator (SOI), III–V semiconductors, glass, and polymers.

Broadly defined, an optical resonator is a structure which confines light in all spatial directions. In a microring resonator, this is achieved in two ways: transversely by the refractive index contrast of the dielectric waveguide used to form the microring and longitudinally by the periodic boundary condition imposed by the ring or racetrack structure. The propagation characteristics of the dielectric waveguide, and especially those of the curved waveguide, thus have a major impact on the characteristics of the microring

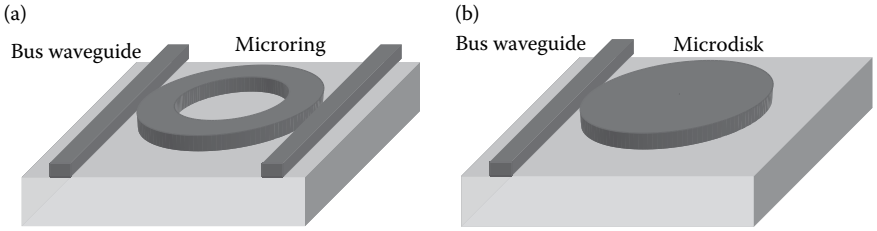

Figure 1.1 Schematic of (a) a microring resonator coupled to two bus (or access) waveguides and (b) a microdisk resonator coupled to one bus waveguide.

resonator. In addition, the manner by which light is coupled into and out of the resonator is also of practical importance. Typically this is achieved via evanescent field coupling between the microring waveguide and one or two external straight waveguides, called access or bus waveguides, by which light is coupled into or out of the resonator. Figure 1.1 illustrates a microring resonator coupled to two bus waveguides and its microdisk variant coupled to a single waveguide.

This chapter provides a brief review of the basic elements constituting a microring resonator, with a view on how their designs and properties may affect the performance of the resonator. Section 1.1 reviews the theory of planar dielectric waveguides and the wave equations governing optical mode propagation. Section 1.2 looks at light propagation in curved waveguides and examines the properties of whispering gallery modes in microdisk and microring resonators. Section 1.3 develops a formalism for analyzing the coupling of waveguide modes in space, which is useful for designing evanescent wave couplers for coupling light into and out of a microring resonator. Finally, Section 1.4 provides an overview of standard fabrication processes for microring devices and highlights several important issues relevant to the practical implementation of these devices.

1.1 Dielectric Optical Waveguides

Dielectric optical waveguides are the basic structures for confining and guiding light in well-defined discrete modes in photonic integrated circuits (PICs). A planar dielectric waveguide consists of a core of refractive index n_1 embedded in other dielectric layers

of lower refractive indices. Light is confined within the core due to total internal reflection at the interfaces between the high-index core and the lower-index cladding media. The degree of confinement increases with the refractive index contrast between the core and cladding. For a waveguide with a uniform cladding of refractive index n_2, the index contrast is defined as

$$\Delta n = \frac{n_1^2 - n_2^2}{2n_1^2} \approx \frac{n_1 - n_2}{n_1}. \tag{1.1}$$

The approximation in the above formula is good for low-index contrast waveguides. Some common waveguide material systems and their index contrasts are listed in Table 1.1. Typically, the index contrast ranges from about 1% for weakly confined waveguides based on doped silica materials, to over 40% for strongly confined semiconductor waveguides. In general, high-index contrast (or high-Δn) waveguides are desirable for the miniaturization of PICs since they have smaller dimensions and provide stronger confinement of light, which enables sharp waveguide bends to be realized with low bending loss. On the other hand, polarization-dependent effects and scattering loss also tend to be more pronounced in high-Δn waveguides.

Two basic optical waveguide structures are shown in Figure 1.2: the rib (or ridge) waveguide and the rectangular strip waveguide. From the fabrication point of view, these two structures differ only by the etch depth in defining the waveguide core: in a rib waveguide, the core is etched only to a depth h leaving a residual high-index

Table 1.1 Refractive Indices of Some Common Integrated Optic Waveguide Materials

Core Material	**Refractive Index at $\lambda = 1.55$ μm**	**Index Contrast[a] Δn (%)**
Doped silica	1.45–1.5	0.7–4
Polymers	1.45–1.7	0.7–14
SiO_xN_y	1.45–2.0	0.7–24
SiN_x	2.0–2.3	24–30
III–V (InP, GaAs)	3.16, 3.4	40, 41
Si	3.47	41

[a] Index contrast assuming SiO_2 cladding with refractive index $n_2 = 1.44$.

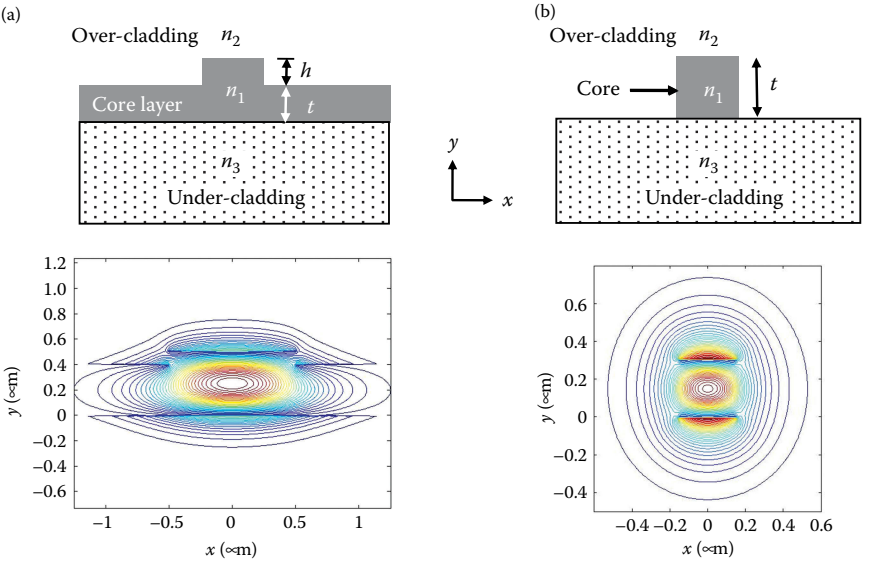

Figure 1.2 Schematic and E_y-field distribution of the quasi-TM mode of (a) a rib (or ridge) waveguide and (b) a rectangular strip waveguide.

layer of thickness t, whereas in a strip waveguide, the core layer is completely etched through. However, the modal characteristics of the two waveguides are quite different, as shown in Figure 1.2. In the rib waveguide, the residual high-index layer causes the mode to expand laterally. Due to the weak lateral confinement, rib waveguides tend to suffer from larger bending loss than strip waveguides. As a result, microring resonators are typically designed using strip waveguides to minimize radiation loss due to bending.

Since the performance of a PIC (photonic integrated circuit) depends critically on the properties of the waveguide modes, it is important to obtain a detailed analysis of the propagation characteristics of light in the optical waveguide. In the next section, we will derive the wave equation and its various approximations for describing electromagnetic wave propagation in a planar dielectric waveguide. A review of the main methods for solving these equations will also be given.

1.1.1 The vectorial wave equations

The field distributions of a waveguide mode and its associated propagation constant are determined by solving an eigenvalue problem formulated in terms of either the transverse electric (TE)

field or transverse magnetic (TM) field. We consider a dielectric waveguide oriented along the z-axis and characterized by a transverse index profile $n(x, y)$. Under the assumption that the transverse index profile is invariant along the propagation axis (the z-axis), the electric and magnetic field distributions of a waveguide mode can be expressed as

$$\boldsymbol{\mathcal{E}}(x,y,z) = \mathbf{E}(x,y)e^{-j\beta z}, \tag{1.2}$$

$$\boldsymbol{\mathcal{H}}(x,y,z) = \mathbf{H}(x,y)e^{-j\beta z}, \tag{1.3}$$

where β is the propagation constant of the waveguide mode and the time dependence $e^{j\omega t}$ is assumed and suppressed. For the purpose of modal analysis, it is convenient to further decompose the fields $\mathbf{E}$ and $\mathbf{H}$ into a transverse component and a longitudinal component as follows:

$$\mathbf{E}(x,y) = \mathbf{E}_t(x,y) + E_z(x,y)\hat{\mathbf{z}}, \tag{1.4}$$

$$\mathbf{H}(x,y) = \mathbf{H}_t(x,y) + H_z(x,y)\hat{\mathbf{z}}. \tag{1.5}$$

The electric and magnetic fields $\boldsymbol{\mathcal{E}}$ and $\boldsymbol{\mathcal{H}}$ satisfy Maxwell's equations,

$$\nabla \times \boldsymbol{\mathcal{E}} = -j\omega\mu_0 \boldsymbol{\mathcal{H}}, \tag{1.6}$$

$$\nabla \times \boldsymbol{\mathcal{H}} = j\omega\varepsilon_0 n^2(x,y)\boldsymbol{\mathcal{E}}, \tag{1.7}$$

where ε_0 and μ_0 are the electric permittivity and magnetic permeability, respectively, of vacuum. By taking the curl of Equation 1.6 and using Equation 1.7 to eliminate $\nabla \times \boldsymbol{\mathcal{H}}$ from the resulting equation, we get

$$\nabla \times \nabla \times \boldsymbol{\mathcal{E}} = n^2 k^2 \boldsymbol{\mathcal{E}}, \tag{1.8}$$

where $k = \omega/c$. With the help of the vector identity $\nabla \times \nabla \times \boldsymbol{\mathcal{E}} = \nabla(\nabla \cdot \boldsymbol{\mathcal{E}}) - \nabla^2 \boldsymbol{\mathcal{E}}$, we can write Equation 1.8 as

$$\nabla^2 \boldsymbol{\mathcal{E}} + n^2 k^2 \boldsymbol{\mathcal{E}} = \nabla(\nabla \cdot \boldsymbol{\mathcal{E}}). \tag{1.9}$$

Substituting $\boldsymbol{\mathcal{E}}(x,y,z) = \mathbf{E}(x,y)e^{-j\beta z}$ into the above equation and making use of the field decomposition in Equation 1.4, we obtain

$$\nabla_t^2 \mathbf{E}_t + (n^2 k^2 - \beta^2)\mathbf{E}_t = \nabla_t(\nabla_t \cdot \mathbf{E}_t) + \nabla_t\left(\frac{\partial E_z}{\partial z}\right), \tag{1.10}$$

where $\nabla_t = \hat{\mathbf{x}}(\partial/\partial x) + \hat{\mathbf{y}}(\partial/\partial y)$. In the absence of free charge, Gauss's law gives

$$\nabla \cdot (n^2 \mathbf{E}) = \nabla_t \cdot (n^2 \mathbf{E}_t) + n^2 \frac{\partial E_z}{\partial z} = 0, \tag{1.11}$$

from which we get

$$\frac{\partial E_z}{\partial z} = -\frac{1}{n^2}\nabla_t \cdot (n^2 \mathbf{E}_t). \tag{1.12}$$

Upon substituting the above expression into Equation 1.10, we obtain the vectorial wave equation in terms of the transverse electric field,

$$\nabla_t^2 \mathbf{E}_t + (n^2 k^2 - \beta^2)\mathbf{E}_t = \nabla_t(\nabla_t \cdot \mathbf{E}_t) - \nabla_t\left[\frac{1}{n^2}\nabla_t \cdot (n^2 \mathbf{E}_t)\right]. \tag{1.13}$$

Equation 1.13 is an eigenvalue problem whose solution gives the transverse field distribution $\mathbf{E}_t$ of an optical mode and its propagation constant β. The effective index of the waveguide mode is defined as $n_{\text{eff}} = \beta/k$.

The terms on the right-hand side of Equation 1.13 account for the polarization coupling between the transverse field components E_x and E_y. Thus, in general, the mode of an optical waveguide is hybrid or vectorial in nature, that is, it contains both E_x and E_y components of the electric field. We can write Equation 1.13 in the form of an eigenvalue matrix equation as (Xu et al. 1994)

$$\begin{bmatrix} P_{xx} & P_{xy} \\ P_{yx} & P_{yy} \end{bmatrix}\begin{bmatrix} E_x \\ E_y \end{bmatrix} = \beta^2 \begin{bmatrix} E_x \\ E_y \end{bmatrix}, \tag{1.14}$$

where the operators in the matrix are given by

$$P_{xx}E_x = \frac{\partial}{\partial x}\left[\frac{1}{n^2}\frac{\partial}{\partial x}\left(n^2 E_x\right)\right] + \frac{\partial^2 E_x}{\partial y^2} + n^2 k^2 E_x, \tag{1.15}$$

$$P_{yy}E_y = \frac{\partial^2 E_y}{\partial x^2} + \frac{\partial}{\partial y}\left[\frac{1}{n^2}\frac{\partial}{\partial y}\left(n^2 E_y\right)\right] + n^2 k^2 E_y, \tag{1.16}$$

$$P_{xy}E_y = \frac{\partial}{\partial x}\left[\frac{1}{n^2}\frac{\partial}{\partial y}\left(n^2 E_y\right)\right] - \frac{\partial^2 E_y}{\partial y \partial x}, \tag{1.17}$$

$$P_{yx}E_x = \frac{\partial}{\partial y}\left[\frac{1}{n^2}\frac{\partial}{\partial x}\left(n^2 E_x\right)\right] - \frac{\partial^2 E_x}{\partial x \partial y}. \tag{1.18}$$

It is apparent from Equation 1.14 that the operators P_{xy} and P_{yx} give rise to polarization coupling effects. For rectangular waveguides with low to moderate index contrasts, the two lowest-order modes are predominantly linearly polarized along either the principal *x*- or *y*-axis. It is often a good approximation to neglect the minor field component of each mode and consider the mode to be either quasi-TE with major field component E_x, or quasi-TM with major field component E_y. Under this semi-vectorial approximation, the cross-polarization coupling terms in Equation 1.14 are neglected so that the equations governing the major field components become

$$P_{xx}E_x = \frac{\partial}{\partial x}\left[\frac{1}{n^2}\frac{\partial}{\partial x}\left(n^2 E_x\right)\right] + \frac{\partial^2 E_x}{\partial y^2} + n^2 k^2 E_x = \beta_{TE}^2 E_x, \quad \text{(quasi-TE)} \tag{1.19}$$

$$P_{yy}E_y = \frac{\partial^2 E_y}{\partial x^2} + \frac{\partial}{\partial y}\left[\frac{1}{n^2}\frac{\partial}{\partial y}\left(n^2 E_y\right)\right] + n^2 k^2 E_y = \beta_{TM}^2 E_y. \quad \text{(quasi-TM)} \tag{1.20}$$

For low-index contrast waveguides, one may further neglect the spatial index variation in the square bracket terms in the above equations. Under this approximation, the TE and TM modes become identical and are described by the scalar wave equation

$$P_{xx}E = P_{yy}E = \frac{\partial^2 E}{\partial x^2} + \frac{\partial^2 E}{\partial y^2} + n^2 k^2 E = \beta^2 E. \tag{1.21}$$

Figure 1.3 shows the electric field distributions of the two lowest-order modes in an SOI strip waveguide consisting of a Si core of 250 nm thickness and 400 nm width embedded in a SiO_2 cladding. Both the semi-vectorial and full-vectorial solutions of the modes are shown for comparison. Also shown are the effective indices of the modes at the 1.55 μm wavelength. We see that the semi-vectorial and full-vectorial solutions give similar field distributions

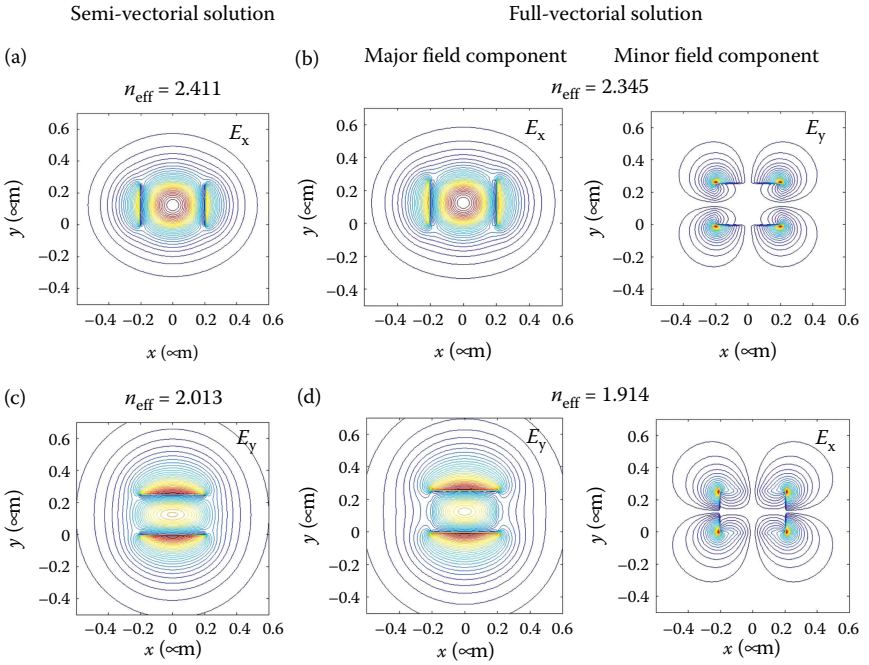

Figure 1.3 Semi-vectorial and full-vectorial solutions of the two lowest-order modes at 1.55 μm wavelength of an SOI strip waveguide (Si core of dimensions 400×250 nm^2 embedded in a SiO_2 cladding): (a, b) TE mode, (c, d) TM mode.

for the major field component of each mode, although there is a difference of about 3–5% between the effective index values.

We can also formulate the wave equation in terms of the transverse magnetic field $\mathbf{H}_t$. One advantage of solving for the optical mode in terms of the magnetic field is that the fields H_x and H_y are continuous across all dielectric boundaries. By taking the curl of Equation 1.7 and using Equation 1.6 to eliminate $\nabla \times \boldsymbol{\mathcal{E}}$, we get

$$\nabla^2 \boldsymbol{\mathcal{H}} + n^2 k^2 \boldsymbol{\mathcal{H}} = -\frac{1}{n^2} \nabla n^2 \times (\nabla \times \boldsymbol{\mathcal{H}}). \tag{1.22}$$

Substituting Equations 1.3 and 1.5 into the above equation, we obtain the following vectorial wave equation in terms of the transverse magnetic field,

$$\nabla_t^2 \mathbf{H}_t + (n^2 k^2 - \beta^2)\mathbf{H}_t = -\frac{1}{n^2} (\nabla_t n^2) \times (\nabla_t \times \mathbf{H}_t). \tag{1.23}$$

The above equation can be written explicitly in a component form as (Xu et al. 1994)

$$\begin{bmatrix} Q_{xx} & Q_{xy} \\ Q_{yx} & Q_{yy} \end{bmatrix} \begin{bmatrix} H_x \\ H_y \end{bmatrix} = \beta^2 \begin{bmatrix} H_x \\ H_y \end{bmatrix}, \tag{1.24}$$

where

$$Q_{xx}H_x = \frac{\partial^2 H_x}{\partial x^2} + n^2 \frac{\partial}{\partial y}\left(\frac{1}{n^2}\frac{\partial H_x}{\partial y}\right) + n^2 k^2 H_x, \tag{1.25}$$

$$Q_{yy}H_y = n^2 \frac{\partial}{\partial x}\left(\frac{1}{n^2}\frac{\partial H_y}{\partial x}\right) + \frac{\partial^2 H_y}{\partial y^2} + n^2 k^2 H_y, \tag{1.26}$$

$$Q_{xy}H_y = \frac{\partial^2 H_y}{\partial x \partial y} - n^2 \frac{\partial}{\partial y}\left(\frac{1}{n^2}\frac{\partial H_y}{\partial x}\right), \tag{1.27}$$

$$Q_{yx}H_x = n^2 \frac{\partial}{\partial x}\left(\frac{1}{n^2}\frac{\partial H_x}{\partial y}\right) + \frac{\partial^2 H_x}{\partial y \partial x}. \tag{1.28}$$

In general, the vectorial wave equations (1.13) and (1.23) do not have analytical solutions and must be solved numerically. Many efficient numerical techniques have been developed for solving these equations for waveguides with arbitrary cross-sections and index profiles, the most popular ones being the finite difference method (Xu et al. 1994) and the finite element method (Rahman and Davies 1984, Koshiba 1992).[*,†] Approximate methods for computing the effective index are also available, such as Marcatili's method (Marcatili 1969a), the effective index method (EIM) (Knox and Toulios 1970), and perturbation methods (Chiang 1993). These methods generally give good approximations for low index contrast waveguides or for modes far from cutoff. Despite its approximate nature, the EIM has found widespread use in the analysis of planar waveguides, even for high-index contrast waveguides, thanks

[*] The finite element method is typically formulated based on either Equation 1.9 for the electric field or Equation 1.22 for the magnetic field.

[†] Commercial software for computing the field distributions and effective indices of optical waveguide modes are also available, such as COMSOL, RSoft, Optiwave, and Lumerical.

to its simplicity and intuitive approach. Given the importance of the method for waveguide analysis, we will briefly review the key aspects of the EIM method below.

1.1.2 The EIM and solutions of the one-dimensional slab waveguide

The basic idea of the EIM method (Knox and Toulios 1970) is the successive approximations of a two-dimensional (2D) rectangular waveguide by one-dimensional (1D) slab waveguides, which can be separately analyzed. The procedure is illustrated in Figure 1.4 for both a rib waveguide and a strip waveguide. In the first approximation, the vertical index profile in each of the core and cladding regions (regions I and II) is replaced by the effective index of the corresponding 1D, y-confined slab waveguides with y-dependent index profiles. This procedure reduces the 2D waveguide to a 1D, x-confined slab waveguide with an x-dependent effective index distribution $n_{\text{eff}}(x)$. The effective index of the equivalent slab waveguide

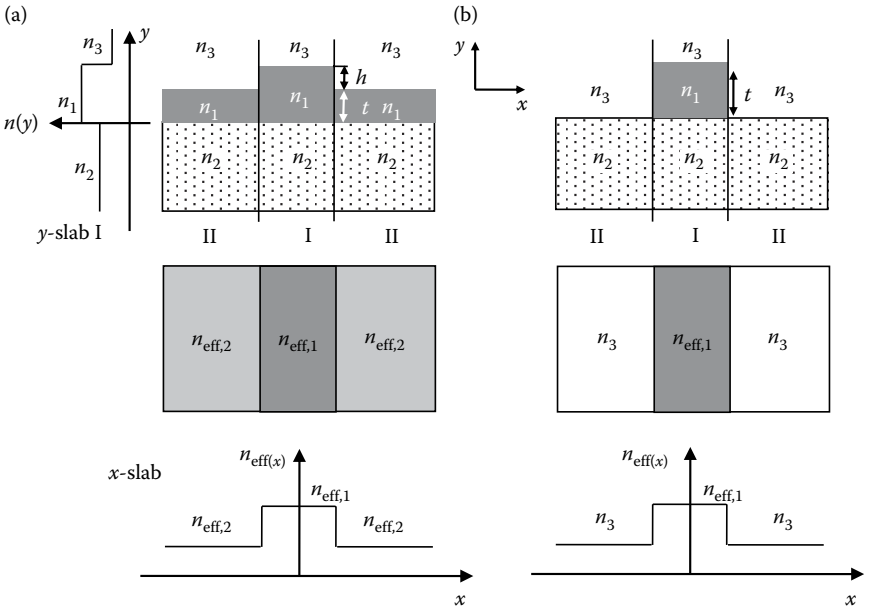

Figure 1.4 Successive approximations of a 2D waveguide by 1D slab waveguides in the EIM: (a) rib waveguide and (b) strip waveguide. The index profile $n(y)$ of the y-confined slab waveguide in the core region (region I) and the effective index distribution $n_{\text{eff}}(x)$ of the x-confined slab waveguide are also shown.

is then determined and taken as an approximation to the effective index of the 2D rectangular waveguide.

The mathematical basis of the EIM method lies in the assumption that the TE and TM semi-vectorial wave equations are separable. For example, for the quasi-TE mode, we assume that the solution for the electric field E_x in Equation 1.19 has the form

$$E_x(x,y) = X(x)Y(y). \tag{1.29}$$

Substituting this solution into Equation 1.19 and dividing by $X(x)Y(y)$, we get

$$\frac{1}{X}\frac{d}{dx}\left[\frac{1}{n^2}\frac{d}{dx}\left(n^2X\right)\right] + \frac{1}{Y}\frac{d^2Y}{dy^2} + (n^2k^2 - \beta_{TE}^2) = 0, \tag{1.30}$$

where $n = n(x, y)$ is the index profile of the 2D waveguide. By adding and subtracting the term $n_{eff}^2(x)k^2$ to Equation 1.30, we can separate it into two 1D wave equations (Okamoto 2000):

$$\frac{d^2Y}{dy^2} + \left[n^2(x,y) - n_{eff}^2(x)\right]k^2Y(y) = 0, \tag{1.31}$$

$$\frac{d}{dx}\left[\frac{1}{n_{eff}^2(x)}\frac{d}{dx}\left(n_{eff}^2(x)X\right)\right] + \left[n_{eff}^2(x)k^2 - \beta_{TE}^2\right]X(x) = 0. \tag{1.32}$$

We recognize Equation 1.31 as the TE wave equation for a y-confined slab waveguide and Equation 1.32 is the TM wave equation for an x-confined slab waveguide. We first solve Equation 1.31 in each of the core and cladding regions (regions I and II) to obtain the lateral effective index distribution $n_{eff}(x)$. The TM effective index of the equivalent x-confined slab waveguide is then determined by solving Equation 1.32. Alternatively, it is more convenient to determine the TM effective index of the x-confined slab waveguide by solving the wave equation in terms of the magnetic field H_y

$$\frac{d^2H_y}{dx^2} + \left[n_{eff}^2(x)k^2 - \beta^2\right]H_y(x) = 0. \tag{1.33}$$

In general, the error in the effective index value obtained by the EIM method arises from two approximations. The first approximation is the use of the semi-vectorial wave equations to approximate

the hybrid modes of the waveguide. The second approximation comes from the fact that in order for the semi-vectorial equation (1.19) or (1.20) to be separable, the index profile of the waveguide must be decomposable in the form (Chiang 1996)

$$n^2(x,y) = n_x^2(x) + n_y^2(y). \tag{1.34}$$

The actual index functions $n_x(x)$ and $n_y(y)$ assumed by the EIM method depend on the waveguide structure being analyzed.

The computation of the effective index of a 2D waveguide by the EIM method reduces to the solution of two 1D slab waveguides. In fact, one of the appealing features of the EIM method is that analytical solutions exist for the TE and TM modes of a 1D slab waveguide. In Table 1.2, we summarize the field solutions and characteristic equations for the TE and TM modes of a general asymmetric slab waveguide with width d and index distribution $n(x)$ shown in Figure 1.5.

Table 1.2 Summary of the Solutions and Characteristic Equations for the TE and TM Modes in an Asymmetric Slab Waveguide

TE Modes	**TM Modes**
Wave Equation	
$\frac{d^2E_y}{dx^2} + [n^2(x)k^2 - \beta^2]E_y = 0$	$\frac{d^2H_x}{dx^2} + [n^2(x)k^2 - \beta^2]H_x = 0$
Field Solution	
$E_y(x,z) = E_0\psi(x)e^{-j\beta z}$	$H_x(x,z) = H_0\psi(x)e^{-j\beta z}$
$\psi(x) = \begin{cases} \cos(k_x d/2 + \theta)e^{-\gamma(x-d/2)}, & x > d/2 \\ \cos(k_x x + \theta), & -d/2 \le x \le d/2 \\ \cos(k_x d/2 - \theta)e^{\alpha(x+d/2)}, & x < -d/2 \end{cases}$	
Characteristic Equation	
$2k_x d - \varphi_1 - \varphi_2 = 2m\pi \quad (m = 0,1,2,3,\ldots)$	
$4\theta = \varphi_1 - \varphi_2$	
$\varphi_1 = 2\tan^{-1}(\alpha/k_x)$	$\varphi_1 = 2\tan^{-1}(n_1^2\alpha/n_2^2k_x)$
$\varphi_2 = 2\tan^{-1}(\gamma/k_x)$	$\varphi_2 = 2\tan^{-1}(n_1^2\gamma/n_3^2k_x)$
$\beta^2 + k_x^2 = n_1^2k^2, \quad \beta^2 - \alpha^2 = n_2^2k^2, \quad \beta^2 - \gamma^2 = n_3^2k^2$	

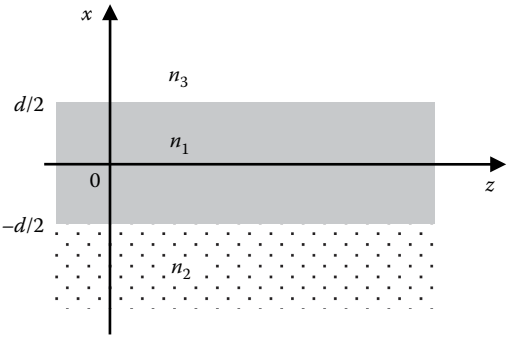

Figure 1.5 Schematic of a 1D asymmetric slab waveguide of width d, core index n_1, lower cladding index n_2, and upper cladding index n_3.

1.1.3 Waveguide dispersion

In general, the effective index of a dielectric waveguide depends on the wavelength so that light at different frequencies propagates at different velocities. This gives rise to dispersion effects such as temporal broadening of a pulse propagating in the waveguide. In a single-mode waveguide, the two main sources of this wavelength dependence (also called intramodal dispersion) are material dispersion and waveguide dispersion. Material dispersion refers to the dependence of the refractive indices of the core and cladding materials on the wavelength. Material dispersion has its physical origin in the dependence of the optical absorption of a material on frequency, so that its permittivity also depends on the frequency through the Kramers–Kronig relation. The dependence of the refractive index of a material on the wavelength can be modeled by the Sellmeier equation

$$n^2(\lambda) = 1 + \sum_i \frac{A_i}{1 - (\lambda_i/\lambda)^2}. \tag{1.35}$$

The coefficients A_i and λ_i for silica and crystalline silicon are given in Table 1.3.

The second source of intramodal dispersion is waveguide dispersion, which is a structural effect and arises from the confinement of light in the waveguide core. In general, strongly confined waveguides exhibit higher waveguide dispersion due to stronger interaction of the mode with the core boundaries. In addition, in a multi-mode waveguide, there exists a third source of dispersion,

Table 1.3 Coefficients of the Sellmeier Equation for SiO_2 and Si

	SiO_2 λ = **0.21–3.71 μm at 295 K** **(Malitson 1965)**	**Si** λ = **1.1–5.6 μm at 295 K** **(Frey et al. 2006)**
A_1	0.6961663	10.67087
A_2	0.4079426	–37.10820
A_3	0.8974794	
λ_1 (μm)	0.0684043	0.3045744
λ_2 (μm)	0.1162414	611.2222
λ_3 (μm)	9.896161	

called intermodal dispersion, which arises from the fact that different waveguide modes have different effective indices and thus propagate at different phase velocities.

The parameter used to quantify the total dependence of the effective index on wavelength is the group index, which is defined as

$$n_g = \frac{d\beta}{dk} = n_{eff} - \lambda_0 \frac{dn_{eff}}{d\lambda}. \tag{1.36}$$

From the group index, we can calculate the group velocity, which is the velocity at which a pulse with a frequency spectrum centered around λ_0 travels in the waveguide,

$$v_g = \frac{d\omega}{d\beta} = \frac{c}{n_g}. \tag{1.37}$$

The group delay experienced by a pulse after propagating a unit distance in the waveguide is given by $\tau_g = 1/v_g = d\beta/d\omega$. To express the fact that the group delay is wavelength dependent, we write τ_g in terms of a Taylor series expansion around the center wavelength λ_0,

$$\tau_g(\lambda) = \tau_g(\lambda_0) + \Delta\lambda \frac{d\tau_g}{d\lambda} + \frac{(\Delta\lambda)^2}{2} \frac{d^2\tau_g}{d\lambda^2} + \cdots \tag{1.38}$$

Defining the total chromatic dispersion of the waveguide as

$$D = \frac{d\tau_g}{d\lambda} = \frac{d}{d\lambda}\left(\frac{n_g}{c}\right) = -\frac{\lambda_0}{c} \frac{d^2 n_{eff}}{d\lambda^2}, \tag{1.39}$$

we can approximate Equation 1.38 by

$$\tau_g(\lambda) \approx \tau_g(\lambda_0) + D\Delta\lambda. \tag{1.40}$$

For a pulse of spectral width $\Delta\lambda$, we obtain from Equation 1.40 the spread in the group delay due to dispersion in the waveguide,

$$\Delta\tau = \tau_g(\lambda) - \tau_g(\lambda_0) \approx D\Delta\lambda. \tag{1.41}$$

Thus the chromatic dispersion D, typically quoted in units of ps/nm/km, gives the delay spread per unit bandwidth per unit length of the waveguide.

Figure 1.6 shows the plots of n_{eff} versus λ for the TE and TM modes of an SOI waveguide consisting of a silicon core of 250 nm thickness and 400 nm width embedded in SiO_2. The group index is calculated to be $n_g = 4.433$ for the TE mode and $n_g = 4.349$ for the TM mode. The chromatic dispersion of the waveguide is $D = -13.29$ ns/nm/km for the TE mode and $D = 0.972$ ns/nm/km for the TM mode. These values represent the total effects of material dispersion in the core and cladding materials as well as the structural

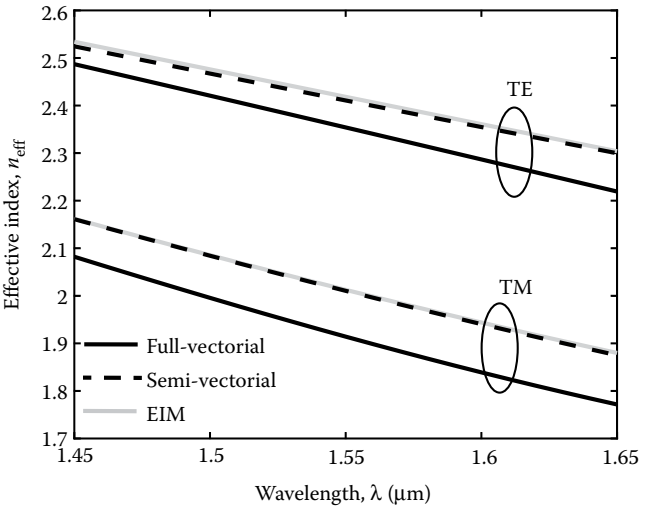

Figure 1.6 Wavelength dependence of the effective index of an SOI waveguide consisting of a silicon core with cross-sectional dimensions 400×250 nm^2 embedded in a SiO_2 cladding.

dispersion of the waveguide. We can also define the chromatic dispersion D_{mat} due to the material alone,

$$D_{mat} = -\frac{\lambda_0}{c}\frac{d^2 n}{d\lambda^2}, \tag{1.42}$$

where $n(\lambda)$ is the bulk index of the material. Near the 1.55 μm wavelength, the material dispersion is −0.862 ns/nm/km for Si and 21.9 ps/nm/km for SiO_2. Comparing these values to the total chromatic dispersion D of the waveguide reveals that waveguide dispersion plays a dominant role in silicon waveguides and indeed in high-index contrast waveguides in general.

It is evident from Figure 1.6 that the effective index also depends on the polarization. In general, the polarization dependence of the effective index arises from the birefringence of the material as well as the geometry of the waveguide. Isotropic materials such as silicon and silica do not have material birefringence, although all materials exhibit some birefringence under thermal or mechanical stress. Thus in a silicon waveguide, the dependence of the effective index on the polarization is a purely structural effect. The total birefringence of a waveguide is defined as the difference between the effective indices of two orthogonal polarization states, commonly chosen to coincide with those of the TE and TM modes:

$$B(\omega) = n_{eff}^{TM}(\omega) - n_{eff}^{TE}(\omega). \tag{1.43}$$

The frequency dependence of the birefringence gives rise to polarization mode dispersion (PMD), which is defined as

$$\text{PMD} = \frac{1}{c}\left|B(\omega) - \omega\frac{dB}{d\omega}\right| \quad (\text{ps/km}). \tag{1.44}$$

The PMD gives the differential time delay between the TE and TM components of a pulse per unit propagating distance.

1.1.4 Propagation loss

There are three main sources of loss in an optical waveguide: optical absorption in the core and cladding materials, electromagnetic scattering, and radiation leakage. Optical absorption arises from various electronic processes in the material such as atomic and molecular

vibrations in glass and polymers, and interband transitions and free carrier absorption (also known as intraband transitions) in semiconductors. Even when the waveguide is operated at a wavelength far from an optical transition, there is still some residual absorption. For example, for bulk crystalline Si, which has a bandgap of 1.1 μm, accurate measurement of the optical absorption constant in a sample with a low impurity concentration of 2×10^{12} cm^3 gives a value of 0.001 dB/cm at 1.55 μm wavelength (Steinlechner et al. 2013).

Loss due to electromagnetic scattering in an optical waveguide is caused by two mechanisms: volume or Rayleigh scattering, and surface roughness scattering. Rayleigh scattering refers to the scattering of light by small fluctuations in the refractive index caused by voids, defects, and contaminants in the material. Rayleigh scattering decreases with wavelength as λ^{-4}, and is typically much smaller than surface roughness scattering. The latter type of scattering refers to the scattering of light due the roughness of waveguide surfaces caused by fabrication processes such as deposition and etching. While the surface roughness due to deposition can be controlled to less than 1 nm, the roughness of the waveguide sidewalls due to dry etching can be as large as a few nanometers. We thus expect to have much larger scattering loss at the waveguide sidewalls than at the top and bottom surfaces of the waveguide core.

In addition to the degree of roughness, surface scattering also depends on the index contrast and how strongly light is confined in the waveguide. Several methods have been developed for estimating waveguide loss due to surface roughness scattering, ranging from the simple model of Tien based on specular reflection (Tien 1971), to more sophisticated models based on the Coupled Mode Theory (CMT) (Marcuse 1969) which take into account the statistical distribution of the roughness. However, since it is difficult to measure the roughness profiles on the sidewalls of a waveguide, the usefulness of these analyses is limited to providing broad estimates of the contributions of surface roughness scattering to the total waveguide loss.

The third major source of waveguide loss is radiation leakage. Radiation leakage arises in waveguide geometries which do not have true eigenmode solutions. The two common types of radiation loss in optical waveguides are bending loss and substrate leakage. Bending loss occurs in curved waveguides and will be discussed in more detail in Section 1.2. Substrate leakage refers to the leakage of light from a waveguide into a high-index substrate. In theory, the evanescent field of a waveguide extends indefinitely into the

undercladding. The presence of a high-index substrate (such as silicon) causes evanescent coupling of light into the substrate which radiates away as loss. Substrate leakage can be minimized by increasing the thickness of the undercladding layer to provide sufficient isolation of the waveguide core from the high-index substrate.

1.2 Optical Modes in Bent Dielectric Waveguides

In a bent dielectric waveguide, the optical mode is pushed toward the outer edge of the waveguide as light propagates around the bend. As the radius of curvature increases, a portion of the evanescent tail of the mode begins to leak out in the form of radiation, resulting in bending loss. A number of techniques have been used to analyze the modes of curved optical waveguides and the associated bending loss. These techniques range from approximate analytical methods such as Marcatili's method (Marcatili 1969b), the conformal mapping method (Heiblum and Harris 1975), to rigorous numerical solutions of the wave equation in cylindrical coordinates (Rivera 1995, Lui et al. 1998, Kakihara et al. 2006). In general, approximate analytical methods give adequately accurate results for curved waveguides with low-index contrasts and large bending radii. For high-index contrast and tightly bent waveguides, the modes become highly hybridized and a full-vectorial numerical solution is required to obtain an accurate analysis of the modal characteristics.

We begin in Section 1.2.1 with an approximate analysis of bent waveguides by the conformal mapping method. Although strictly valid only for 2D structures, the conformal mapping method provides an intuitive understanding of the propagation characteristics and the mechanisms causing radiation loss in curved waveguides. For microdisk and microring structures, analytical solutions for the discrete resonant modes can be obtained by solving the 2D semi-vectorial wave equation in polar coordinates. This is the subject of Section 1.2.2. Finally, Section 1.2.3 will give a full-vectorial formulation of the problem in the three-dimensional (3D) cylindrical coordinate system (CCS) which is suitable for rigorous numerical simulations of bent waveguides.

1.2.1 Conformal transformation of bent waveguides

The idea of the conformal mapping method is to apply a coordinate transformation to the wave equation which will convert the curved

boundaries of the structure in the original (x, y) coordinates into straight boundaries in the new (u, v) coordinates. Conformal mapping is based on the Cauchy–Riemann equations, which are valid for domains in a 2D plane. To apply the method to a 3D curved waveguide, we first reduce the waveguide to an equivalent 2D structure in the x–y plane using the EIM, as shown in Figure 1.7. The semi-vectorial equation governing wave propagation in the 2D bent waveguide is then given by

$$\frac{\partial^2 F}{\partial x^2} + \frac{\partial^2 F}{\partial y^2} + n^2(x,y)k^2 F = 0, \tag{1.45}$$

where $n(x, y)$ is the effective index distribution and

$$F(x,y) = \begin{cases} H_z, & \text{quasi-TE mode,} \\ E_z, & \text{quasi-TM mode.} \end{cases} \tag{1.46}$$

The conformal transformation which converts circular boundaries in the x–y plane into straight boundaries in the u–v plane is (Heiblum and Harris 1975)

$$u = \frac{R_{\text{ref}}}{2} \ln\left(\frac{x^2 + y^2}{R_{\text{ref}}^2}\right) = R_{\text{ref}} \ln\left(\frac{r}{R_{\text{ref}}}\right), \tag{1.47}$$

$$v = R_{\text{ref}} \tan^{-1}\left(\frac{y}{x}\right) = R_{\text{ref}}\theta, \tag{1.48}$$

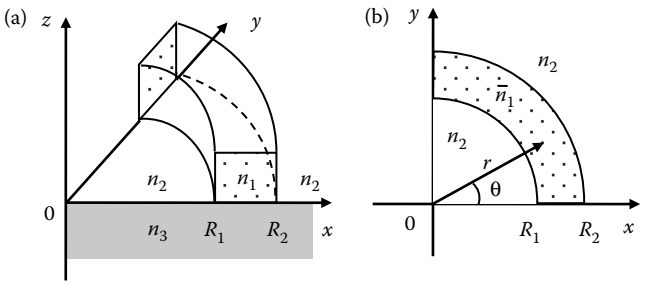

Figure 1.7 Reduction of a 3D bent waveguide in (a) to an equivalent 2D structure in (b) by the EIM. The index n_1 of the core region is replaced by the effective index $\bar{n}_1$ in (b).